Biophysics of Membrane Stiffening by Cholesterol and Phosphatidylinositol 4,5-bisphosphate (PIP2)

Fathima T. Doole, Sudipta Gupta, Teshani Kumarage, Rana Ashkar, and Michael F. Brown

Abstract Cell membranes regulate a wide range of phenomena that are implicated in key cellular functions. Cholesterol, a critical component of eukaryotic cell membranes, is responsible for cellular organization, membrane elasticity, and other critical physicochemical parameters. Besides cholesterol, other lipid components such as phosphatidylinositol 4,5-bisphosphate (PIP2) are found in minor concentrations in cell membranes yet can also play a major regulatory role in various cell functions. In this chapter, we describe how solid-state deuterium nuclear magnetic resonance (^{2}H NMR) spectroscopy together with neutron spin-echo (NSE) spectroscopy can inform synergetic changes to lipid molecular packing due to cholesterol and PIP2 that modulate the bending rigidity of lipid membranes. Fundamental structure–property relations of molecular self-assembly are illuminated and point toward a length and time-scale dependence of cell membrane mechanics, with significant implications for biological activity and membrane lipid–protein interactions.

Keywords Area per lipid · Cholesterol · PIP2 · Membrane elasticity · Membrane viscosity · Neutron spin-echo · Polymer brush model · Solid-state ^{2}H NMR

Authors Fathima T. Doole and Sudipta Gupta have equally contributed to this chapter.

F. T. Doole
Department of Chemistry and Biochemistry, University of Arizona, Tucson, AZ, USA

S. Gupta · T. Kumarage · R. Ashkar (✉)
Department of Physics and Center for Soft Matter and Biological Physics, Virginia Tech, Blacksburg, VA, USA
e-mail: ashkar@vt.edu

M. F. Brown (✉)
Department of Chemistry and Biochemistry, University of Arizona, Tucson, AZ, USA

Department of Physics, University of Arizona, Tucson, AZ, USA
e-mail: mfbrown@u.arizona.edu

Abbreviations

DMPC   1,2-dimyristoyl-*sn*-glycero-3-phosphocholine
DOPC   1,2-dioleoyl-*sn*-glycero-3-phosphocholine
EFG   electric field gradient
FERM   protein 4.1, ezrin, radixin, moesin
LUV   large unilamellar vesicles
MD   molecular dynamics
NMR   nuclear magnetic resonance
NSE   neutron spin-echo
PC   phosphocholine or phosphatidylcholine
POPC   1-palmitoyl-2-oleoyl-*sn*-glycero-3-phosphocholine
POPC-d_{31} 1-perdeuteriopalmitoyl-2-oleoyl-*sn*-glycero-3-phosphocholine
SANS   small-angle neutron scattering
SAXS   small-angle X-ray scattering
ZG   Zilman and Granek

1   Introduction

Lipid bilayers, the primary matrix of cell membranes, serve as the cellular platform for nutrient exchange, protein–cell interactions, and viral budding, among other vital cellular processes. Emergent membrane properties at mesoscopic length scales, such as lipid packing and membrane rigidity, are determined by intermolecular interactions, which also drive various membrane dynamics. Lipid membrane fluctuations correspond to the geometry of interactions and the rates of lipid motions. These dynamics are hierarchical in nature, encompassing segmental lipid fluctuations, molecular diffusion, and elastic membrane deformation (Fig. 1a). Phospholipids (Fig. 1b, c) are the main components of the lipid bilayers of animal cells. Phosphatidylinositol 4,5-bisphosphate (PIP2) is a minor phosphoinositide found in cell membranes (Fig. 1d), which plays important roles in cytoskeletal organization, cell motility, transduction of extracellular signals, regulation of ion channels at the plasma membrane, endocytosis, phagocytosis, and endosome function [1]. Cholesterol, another major lipid component in the cell, has justifiably drawn significant attention in membrane biophysics over the last few decades. Cholesterol (Fig. 1e) is present in large amounts in eukaryotic cells but is absent in prokaryotic cells [2], indicating its important role in cell evolution. In mammalian cells, cholesterol can constitute up to 50 mol% of the total lipids of the plasma membrane [3]. The molecular fraction of cholesterol in different cell membranes is controlled by biosynthesis, efflux from cells, and influx of lipoprotein cholesterol into the cell [4]. Functionally, cholesterol is involved in key biological processes such as cellular homeostasis, steroid and vitamin D synthesis, and the regulation of membrane rigidity and fluidity [5]. Changes in cholesterol level are commonly attributed to variations in membrane properties, stability, and pathology. There are two well-known methods by which cholesterol
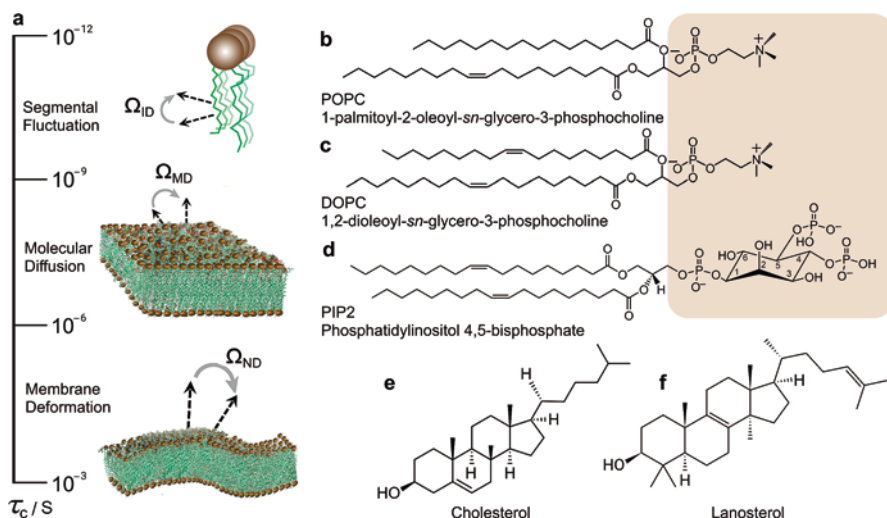
Fig. 1 Mobilities of phospholipids in lipid membranes occur at characteristic time scales. (**a**) Principal axis system (PAS) of $^{13}C-^{1}H$ or $C-^{2}H$ bonds fluctuates due to motions of internal segmental frame (I) with respect to the membrane director axis (D). Diffusive phospholipid motions are described by anisotropic reorientation of molecule-fixed frame (M) with respect to the membrane director axis as described by Ω_{MD} Euler angles. The liquid-crystalline bilayer lends itself to propagation of thermally excited quasi-periodic fluctuations in membrane curvature expressed by motion of the local membrane normal (N) relative to the membrane director axis as described by Ω_{ND} Euler angles. Examples are shown of glycerophospholipids, (**b**) 1-palmitoyl-2-oleoyl-*sn*-glycero-3-phosphocholine (POPC) and (**c**) 1,2-dioleoyl-*sn*-glycero-3-phosphocholine (DOPC); (**d**) PIP2; (**e**) cholesterol, which is the sterol component of animal biomembranes; and (**f**) lanosterol, a precursor in the sterol biosynthesis pathway

modulates cellular functions: (i) indirect regulation of membrane properties (e.g., molecular packing) and subsequent changes to protein–membrane interactions [6–8], or (ii) direct modification of cholesterol–protein interactions [9, 10]. The stiffening effect of cholesterol on both saturated and unsaturated lipid membranes due to changes in lipid packing has been inferred using solid-state nuclear magnetic resonance (NMR) spectroscopy, neutron spin-echo (NSE) spectroscopy, and molecular dynamics (MD) simulations [11, 12]. Changes to lipid molecular packing due to cholesterol interactions with phospholipids such as PIP2 can thus lead to synergistic modulation of the bending rigidity of biomembranes that may affect lipid–protein interactions and underlie the biological functions of both types of lipids.

1.1 Cholesterol and PIP2 Affect Membrane Mechanical Properties

The forces governing the nanoscopic structures of lipid membrane assemblies are described by properties such as the membrane surface tension, area expansion modulus (lateral compressibility), bending rigidity, and the spontaneous curvature.

Generally, lipid–protein interactions and protein function can involve chemically specific interactions and/or nonspecific material properties of the membranes. It is known that cholesterol and PIP2 can control the activity of membrane receptors through specific interactions, and certain proteins have cholesterol-recognition amino acid-consensus (CRAC) motifs [13–15] that involve specific interactions. In addition, cholesterol decreases the activity of proteins and peptides of the innate immune system on liposomal bilayers [16], and formation of the protein 4.1, ezrin, radixin, moesin (FERM) domain/L-selectin complex is favored by PIP2, which clusters about the proteins triggering a conformational transition in the cytoplasmic domain of L-selectin [17]. The other focus is on nonspecific material properties that affect protein–lipid interactions, as in the Fluid-Mosaic Model [18], which describes how the molecules are self-assembled in the membrane. It assumes the lipids and proteins are weakly coupled in the two-dimensional (2D) membrane plane, giving a fluid-like distribution of proteins that undergo rotational and translational diffusion. Alternatively, the lipid–protein interactions are explained by nonspecific material properties using the Flexible Surface Model (FSM) through a balance of curvature and hydrophobic forces [7]. The FSM considers nonspecific bilayer properties involving a two-way elastic coupling of the lipids to the conformational energetics of membrane proteins. The strong out-of-plane proteolipid couplings considered by the FSM affect protein function through elastic forces described by the monolayer spontaneous curvature (H_0) and the Helfrich bending rigidity (κ) [19]. As an example, upon light absorption rhodopsin becomes a sensor of the monolayer spontaneous (intrinsic) curvature, which accounts for the effects of bilayer thickness, nonlamellar-forming lipids, cholesterol, and osmotic stress on its activation [20]. In this chapter, we consider how the average membrane structure, fluctuations, and elastic deformations of the lipids are affected by cholesterol [5].

The structure of cholesterol facilitates the interactions with lipid membranes and its orientation along the hydrocarbon chains of the lipids. Cholesterol orientation in the membrane bilayer results in a more ordered state of the hydrocarbon chains, and consequently modulates the membrane structural, dynamical, and physical properties. Biological membranes contain saturated and unsaturated lipids, where cholesterol favorably separates into domains rich in saturated lipids, also known as lipid rafts. Lipid rafts are important in cell signaling and pharmacology 21– 23], as well as maintaining membrane order [24]. Cholesterol also increases lipid packing, which lowers membrane permeability, affecting the distribution and transport of anesthetics and other drugs in membranes [25, 26]. Therefore, cholesterol also plays a significant regulatory role in many biophysical processes [27], including passive permeation [28], protein and enzyme activity [29, 30], and viral infections, e.g., influenza [31], human immunodeficiency virus (HIV) [32], and coronavirus (severe acute respiratory syndrome-coronavirus-2 [SARS-CoV-2]) [33].

The mechanism by which cholesterol regulates PIP2 varies based on the cell type. For instance, cholesterol depletion in fibroblasts leads to reduced PIP2 concentrations in the plasma membrane, reduced membrane–cytoskeletal attachments, and decreased lateral motility, as reported by Kwik et al. [34]. The same study reports that cholesterol depletion in lymphoblasts results in decreased lateral

mobility of membrane proteins [34]. Similarly, in cultured pancreatic β-cells, cholesterol depletion stimulates the hydrolysis of PIP2, thus reducing the amount of PIP2 at the plasma membrane [35]. However, in another study, Chun et al. report contrasting findings where membrane cholesterol enrichment promoted PIP2 depletion in human embryonic kidney (HEK)293 cells [36]. Likewise, PIP2 lateral mobility has been described as low in atrial myocytes and high in HEK293 cells and fibroblasts [37], suggesting that cholesterol may regulate PIP2 differently in various cell types. Interestingly, the upright straight structure and large headgroup size of PIP2 implies that it may extend further into the aqueous phase than a typical phospholipid [38], potentially altering the assembly or the packing of adjacent lipids. Indeed, Shukla et al. [39] show that PIP2-containing giant unilamellar vesicles can assume a significant spontaneous curvature. They demonstrate that this curvature preference arises from the spontaneous development of trans-bilayer PIP2 asymmetry. Interestingly, similar observations were reported by MD simulation studies that show that compositional asymmetry has a significant effect on calculated membrane properties. Specifically, Jiang et al. report that compared with symmetric POPC bilayers, the addition of 20% PIP2 of negative surface charge in one leaflet of simulated membranes has a minimal effect on the bilayer area compressibility, surface shear viscosity, and bending rigidity [40]. However, the inclusion of 30% cholesterol in PIP2-containing asymmetric bilayers resulted in more than a twofold increase in all three mechanical constants. This opens a potentially interesting synergistic effect between cholesterol and PIP2, which requires further investigation.

For this purpose, the effect of cholesterol on membrane mechanics has been investigated by various techniques, such as flickering spectroscopy [41], micropipette aspiration [42–44], electrodeformation [45, 46], diffuse X-ray scattering [47], MD simulations [48–50], solid-state ^{2}H NMR [51, 52], and neutron spin-echo (NSE) spectroscopy [11, 53]. Among these techniques, NSE spectroscopy, solid-state ^{2}H NMR spectroscopy, and MD simulations are techniques that access mesoscale bending fluctuations. Solid-state ^{2}H NMR spectroscopy and MD simulations give atomistic information, and furthermore NSE spectroscopy directly probes membrane dynamics over length scales ranging from tens to hundreds of angstroms and time scales from 10 ps to 100 ns. A limitation of NSE and ^{2}H NMR is that they cannot provide direct visualization of membrane fluctuations, and instead require model-dependent fitting. By contrast, other biophysical techniques like micropipette aspiration, electrodeformation, and diffuse X-ray scattering report on larger distance scales. An additional advantage of micropipette aspiration [54] and electrodeformation [45] techniques is that they can provide visualization and measure the bilayer deformation directly. In this chapter, we discuss the powerful combination of solid-state ^{2}H NMR and NSE spectroscopy [11, 55], which uniquely access collective lipid fluctuations over length and time scales that are commensurate with key biological processes, including protein–membrane interactions and signaling events. Here we summarize the basic principles of the two techniques and how they can be used to study membrane fluctuations caused by cholesterol as a framework for investigating synergistic interactions of PIP2 with cholesterol in lipid membranes.

2 Introduction to Solid-State NMR Spectroscopy

Using solid-state ^{2}H nuclear magnetic resonance (^{2}H NMR) spectroscopy, we study the spectra and relaxation times of deuterium spin labels in hydrocarbon chains of the lipid molecules under the influence of a magnetic field. Solid-state ^{2}H NMR spectroscopy determines the structure and dynamics of solids and semi-solids [56] and is one of the leading biophysical techniques applicable to lipid bilayers and biomembranes [57]. It gives information about the molecular organization of lipids within membranes, including the structure, ordering, and rates of molecular motions. Atomistically resolved information about collective membrane dynamics, such as elastic deformations of the acyl chain region within the membrane, can be investigated using solid-state ^{2}H NMR order parameter measurements in conjunction with nuclear spin relaxation experiments. The membrane elastic deformations together with their multiscale molecular dynamics fall in the solid-state ^{2}H NMR time and length scales, which allow for a detailed analysis of membrane fluctuations in the presence of cholesterol.

The coupling interactions in solid-state ^{2}H or ^{13}C NMR are sensitive to both orientation and/or distance, and their values correspond to the average structure of the system under study. In the case of ^{2}H NMR spectroscopy, investigating the individual C–^{2}H bonds provides atomic-level details for noncrystalline amorphous or liquid-crystalline systems. The relaxation parameters derived from solid-state ^{2}H NMR spectroscopy give important insights into the relevant molecular motions. One of the distinctive features in solid-state ^{2}H NMR of biomolecular systems is that both line shape data [55] and relaxation times [58] are accessible. The information obtained using this approach involves molecular motions over a range of time scales. Experimental measurements of residual quadrupolar couplings (RQCs) and relaxation rates provide information of the geometry and allow investigations of multiscale molecular motions and their amplitudes in the membrane systems of interest.

2.1 Principles of Solid-State ^{2}H NMR Spectroscopy

Before we apply the technique, understanding the basics of ^{2}H NMR spectroscopy will guide us on the information that is derived. The ^{2}H nucleus possesses a spin of $I = 1$, which gives rise to three Zeeman energy levels. According to quantum mechanics, the Hamiltonian $\hat{H}_Z$ for the interaction of the nuclear magnetic moment with the static magnetic field gives rise to three eigenstates $|m\rangle = |0\rangle$ and $|\pm 1\rangle$. Shifts between adjacent spin energy levels are allowed, producing two single-quantum nuclear spin transitions. The perturbing Hamiltonian $\hat{H}_Z$ represents the interaction of the quadrupole moment of the ^{2}H nucleus with the electric field gradient (EFG) of the C–^{2}H bond of the labeled lipid. For each of the inequivalent sites, two spectral branches are seen in the experimental spectrum. In solid-state ^{2}H NMR

spectroscopy, the experimentally observed quadrupolar coupling is given by the difference in the frequencies $\Delta v_Q^{\pm} \equiv v_Q^+ - v_Q^-$ of the spectral lines due to the perturbing Hamiltonian. The experimental quadrupolar splitting is thus obtained as:

$$\Delta v_Q = \frac{3}{2} \chi_Q D_{00}^{(2)}(\Omega_{PL}), \tag{1}$$

Here, $\chi_Q \equiv e^2 qQ/h$ is the static quadrupolar coupling constant, $D_{00}^{(2)}(\Omega_{PL})$ is a Wigner rotation matrix element, and $\Omega_{PL} \equiv (\alpha_{PL}, \beta_{PL}, \gamma_{PL})$ are the Euler angles [55, 59] relating the principal axis system (PAS) of the EFG tensor (P) to the laboratory frame (L) [60–62].

In liquid-crystalline membranes, the molecular motions are often cylindrically symmetric about the bilayer normal, an axis called the director. The rotation of the principal axis system of the coupling tensor to the laboratory frame is described by the three Ω_{PL} Euler angles (see above), and can thus be represented by two consecutive rotations. First, the Euler angles $\Omega_{PD}(t)$ represent the (time-dependent) rotation from the principal axis frame to the director frame, and second, the Euler angles Ω_{DL} represent the (static) rotation from the director frame to laboratory frame. Use of the closure property of the rotation group [62] is helpful in this regard. Considering the cylindrical symmetry about the director, we can then expand Eq. (1), which now reads:

$$\Delta v_Q = \frac{3}{2} \chi_Q \left\langle D_{00}^{(2)}(\Omega_{PD}) \right\rangle D_{00}^{(2)}(\Omega_{DL}), \tag{2a}$$

$$= \frac{3}{2} \chi_Q \frac{1}{2} \left\langle 3\cos^2 \beta_{PD} - 1 \right\rangle \frac{1}{2} \left(3\cos^2 \beta_{DL} - 1 \right). \tag{2b}$$

Here, $\beta_{DL} \equiv \theta$ is the angle the bilayer normal makes to the static external magnetic field. The segmental order parameter S_{CD} is given by:

$$S_{CD} = \frac{1}{2} \left\langle 3\cos^2 \beta_{PD} - 1 \right\rangle, \tag{3}$$

where the angular brackets denote a time or ensemble average. It follows that

$$\Delta v_Q = \frac{3}{2} \chi_Q S_{CD} P_2 (\cos \beta_{DL}) \tag{4}$$

in which $P_2 (\cos \beta_{DL}) \equiv (3\cos^2 \beta_{DL} - 1)/2$ is the second-order Legendre polynomial. The above formula shows how the quadrupolar splitting depends on the (Euler) angles that rotate the coupling tensor from its principal axes system to the laboratory frame of the main magnetic field [55].

Next, the fluctuations of the coupling Hamiltonian due to the various motions of the lipid molecules within the bilayer give rise to transitions between the various

adjacent energy levels [62]. In solid-state ^{2}H NMR relaxometry of liquid-crystalline membrane lipids, we are typically interested in the spin-lattice (R_{1Z}) relaxation rates. Experimental measurements of the R_{1Z} relaxation rate involve inverting (flipping) the magnetization, and then following the attainment of equilibrium through its recovery as a function of time. The observable relaxation rates are related to the spectral densities of motion in the laboratory frame by the following expression:

$$R_{1Z} = \frac{3}{4}\pi^2 \chi_Q^2 \left[J_1(\omega_0) + 4J_2(2\omega_0) \right]. \tag{5}$$

In this formula, R_{1Z} is the spin-lattice (longitudinal) relaxation rate, $J_m(\omega_0)$ indicates the spectral densities of motion, where $m = 1, 2$, and ω_0 is the deuteron Larmor frequency. The spectral densities $J_m(\omega_0)$ describe the power spectrum of the motions as a function of frequency ω_0 in terms of the fluctuations of the Wigner rotation matrix elements for transforming the coupling (EFG) tensor from its principal axis system within the lipid molecule to the laboratory frame. They are the Fourier transform partners of the orientational correlation functions $G_m(t)$, which depend on time and thereby characterize the C–^{2}H bond fluctuations of the lipids as an experimental window into their molecular dynamics.

Notably, the segmental order parameters depend only on the amplitudes of the C–^{2}H bond motions, while the relaxation rates also depend on the fluctuation rates of the C–^{2}H bond. We have developed a generalized model-free (GMF) approach of relaxation rate analysis [62, 63] that results in a simple dependence of the R_{1Z} rates on the squared segmental order parameters (S_{CD}^2) (square-law) along the chain. For short-wavelength collective lipid excitations, about the bilayer thickness and less, the spectral density reads [64]:

$$J_m(\omega) = \frac{5}{2} S_{CD}^2 D \omega^{-(2-d/2)} \left[\left| D_{-1m}^{(2)}(\beta_{DL}) \right|^2 + \left| D_{1m}^{(2)}(\beta_{DL}) \right|^2 \right]. \tag{6}$$

Here, ω is the angular frequency, D is the viscoelastic constant, d is the dimensionality, and $\mathbf{D}^{(2)}$ indicates the second-rank Wigner rotation matrix [59]. The spectral densities of motion $J_m(\omega)$ depend on the square of the observed S_{CD} order parameters, and the slope of the square-law plot is inversely related to the softness of the membrane. For three-dimensional (3D) quasi-elastic fluctuations, the viscoelastic constant is given by $D = 3k_B T \sqrt{\eta} / 5\pi \sqrt{2K^3 S_s^2}$, where a single elastic constant K is assumed. In this expression, η is the corresponding viscosity coefficient, S_s is the order parameter for the collective slow motions, k_B is the Boltzmann constant, and T is the absolute temperature. Here we assume a single elastic constant, and we do not distinguish between splay, twist, and bend deformations [51]. In addition to the bending modulus κ, the compression modulus K_B comes into play [65]. For splay deformations, the bending rigidity is: $\kappa \approx Kt$, where $t = 2D_C$ is the bilayer thickness, giving a $\kappa^{-3/2}$ dependence of the spin-lattice R_{1Z} rates [66], hence providing knowledge of the bilayer elasticity.

2.2 Membrane Bilayer Properties by Solid-State ^{2}H NMR Spectroscopy

Representative applications of solid-state ^{2}H NMR spectroscopy to lipid membranes include the influence of cholesterol [66–68] as well as acyl chain unsaturation. To determine the average membrane structure, fluctuations, and elastic deformations due to cholesterol, the first-order mean-torque model (Fig. 2a) is instrumental. This model provides two important structural parameters for lipid bilayers: the average area per acyl chain $\langle A \rangle$, and D_C, the hydrophobic thickness of one bilayer leaflet (Fig. 2b). Details of the theory of the first-order mean-torque model have been previously reviewed [69]. The earlier studies by Bartels et al. [70] found striking differences in chain packing for 1-perdeuteriopalmitoyl-2-oleoyl-*sn*-glycero-3-phosphocholine (POPC-d_{31}) upon interaction with cholesterol in binary mixtures (Fig. 2c). They observed that acyl chains of the glycerophospholipid were not affected as strongly as the sphingolipid by the rigid sterol backbone at low cholesterol concentrations [70]. In addition, a more continuous dependence of chain order on cholesterol concentration became observable in the case of 1-palmitoyl-2-oleoyl-*sn*-glycero-3-phosphocholine (POPC). This is obviously due to the less favorable interaction of the unsaturated acyl chain of POPC with cholesterol, as has already been shown for various unsaturated lipids [71–73].

2.3 Membrane Rigidity by Solid-State ^{2}H NMR Spectroscopy

Cholesterol is a steroid molecule, which is amphiphilic in nature. Now let us see the membrane structural deformation and emergent fluctuations at an atomistic level in the presence of cholesterol. For site-specifically labeled phospholipids (or with perdeuterated chains), we de-Pake (deconvolute) the powder-type spectra of random multilamellar dispersions. This provides us with highly resolved subspectra corresponding to the $\theta = 0°$ bilayer (director) orientation (Fig. 3a). These highly resolved signals clearly indicate a gradual increase in the splittings (Δv_Q) with increasing cholesterol content (mol%) where POPC-d_{31} is introduced as a probe lipid (Fig. 3a). Larger residual quadrupolar splittings (Δv_Q) indicate a smaller number of degrees of freedom of the flexible phospholipids which is reduced due to interaction with the rigid cholesterol molecules.

Revisiting Eq. [4], it is evident that the observed residual quadrupolar coupling Δv_Q is directly related to the segmental order parameter S_{CD}. The variations of residual quadrupolar couplings give a profile of the absolute segmental order parameter $S_{CD}^{(i)}$ as a function of chain position (index i). This striking inequivalence comes from the effects of the bilayer packing on the *trans–gauche* isomerization of the acyl groups. Figure 3b shows the segmental order parameters $S_{CD}^{(i)}$, plotted as a function of the acyl position (index i) for 1,2-dioleoyl-*sn*-glycero-3-phosphocholine (DOPC) alone and DOPC in the presence of cholesterol. The plateau region in the
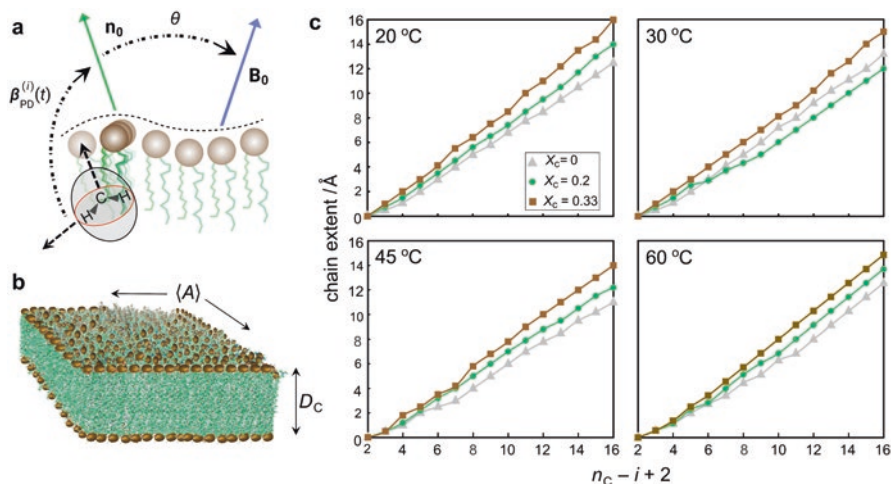
Fig. 2 Bilayer dimensions are given by the interfacial membrane area per lipid $\langle A \rangle$ and the volumetric thickness D_C. (**a**) Schematic representation of methylene chain travel from the lipid headgroup–water interface. Orientation of CH_2 segments and their projection onto the bilayer normal (n_0) are shown in the diagram. (**b**) Structural parameters $\langle A \rangle$ and D_C are calculated from the acyl chain volume V_C and moments $\langle \cos \beta \rangle$ and $\langle \cos^2 \beta \rangle$, obtained from the order parameter plateau, where β is the angle between the virtual bond connecting two neighboring carbons of the ith segment and n_0. (**c**) Chain-extension profiles (cumulative segmental projections) for POPC-d_{31}/cholesterol binary mixtures show the influence of cholesterol on the orientational order of POPC-d_{31} acyl groups. The indexing ($n_C - i + 2$) begins with the terminal methyl group ($i = n_C$) and ends at the C2 carbon ($i = 2$). Results are shown for pure POPC-d_{31} (▲), POPC-d_{31} with $X_C = 0.2$ (●), and POPC-d_{31} with $X_C = 0.33$ (■) at temperatures of 20, 30, 45, and 60 °C. (Figure is adapted from Ref. [70] and redrawn)

order profiles (Fig. 3b) can be explained by the preferred configurations of the acyl chains parallel to the membrane normal. As shown in the figure, the smaller absolute $S_{CD}^{(i)}$ values for DOPC in the absence of cholesterol manifest the additional degrees of freedom of the unsaturated acyl chains.

To explain the relaxation times of lipid bilayers, the ordering and rate of motion must be distinguished as in [74]. In ^2H NMR spectroscopy of membranes, the measurements comprise the order parameter and the relaxation rate profiles. This dependence results in a signature of collective slow bilayer motions that modulate the residual coupling tensors of the local segmental motions. Given that a membrane deformation model applies [75, 76], the R_{1Z} rates illuminate a broad spectrum of 3D collective bilayer excitations along with effective rotations of the lipids. Transverse ^2H NMR spin relaxation studies likewise provide evidence for 2D collective motions of the lipid membrane at lower frequencies [77–82]. Investigations of the influences of both cholesterol and lanosterol on the physical properties of 1,2-diperdeuterio-myristoyl-sn-glycero-3-phosphocholine (DMPC-d_{54}) bilayers at the atomistic level have been conducted using solid-state ^2H NMR spectroscopy (Fig. 4a, b). As in the case of DOPC membranes, a gradual increase in the quadrupolar splittings ($\Delta \nu_Q$) for the acyl segments is seen as the cholesterol concentration is increased, reflecting a
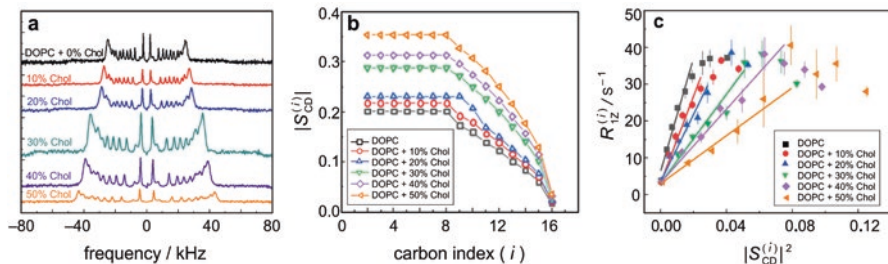
Fig. 3 Interaction with the rigid cholesterol molecules increases the ordering in unsaturated DOPC lipid membranes. (**a**) De-Paked solid-state ^{2}H NMR spectra of DOPC/cholesterol membranes containing 10 mol% of POPC-d_{31} as a probe lipid show greater quadrupolar splittings with increasing cholesterol fraction. (**b**) Segmental order parameter versus acyl position for POPC-d_{31} probe lipid in DOPC/cholesterol membranes with different mol% cholesterol at $T = 25\,°C$. (**c**) Dependence of spin-lattice relaxation rate $R_{1Z}^{(i)}$ on squared order parameters $S_{CD}^{(i)}$ indicating a decrease in square-law slopes due to bilayer stiffening by cholesterol. (Adapted from Ref. [11])

larger orientational order of the acyl chain segments versus the bilayer normal. Immediately this finding explains the well-known condensing effect of cholesterol at the molecular level, involving a decrease of the area per phospholipid molecule at the aqueous interface, accompanied by greater bilayer hydrocarbon thickness. Experimental solid-state ^{2}H NMR relaxation studies of the effect of cholesterol on lipid bilayers further show a square-law dependence of the R_{1Z} rates versus the order parameters S_{CD} along the entire acyl chain for the multilamellar dispersions of DMPC-d_{54}/cholesterol bilayers (Fig. 4a, b). Notably, the square-law functional dependence [83] is a model-free correlation among the experimental observables (Figs. 3c and 4a, b). The progressive increase in the bilayer rigidity of DMPC lipid bilayers obtained by solid-state ^{2}H NMR relaxation at various compositions of DMPC and cholesterol is manifested by the square-law slope (Fig. 4b). According to Fig. 4b both cholesterol and lanosterol decrease the square-law slopes, corresponding to a progressive reduction in bilayer elasticity (Figs. 3c and 4a, b). By contrast, local *trans–gauche* isomerizations along the chain do not yield such a square-law as indicated for DOPC/cholesterol membranes. We attribute this reduction of the square-law slope (Fig. 4b) to an increase in bending rigidity κ due to short-range cholesterol–phospholipid interactions, showing us how membrane mechanical properties begin to emerge from the local atomistic interactions within the lipid bilayer.

3   Introduction to Neutron Spin-Echo Spectroscopy

We next turn to the complementary approach involving neutron spin-echo spectroscopy, which like solid-state ^{2}H NMR rests upon changes in the spin state of scattered neutrons. As a result, we can use a similar strategy in both cases to inform us how the structural and dynamical properties of the lipids are connected with the bilayer composition. Neutron spin-echo (NSE) spectroscopy involves the change in
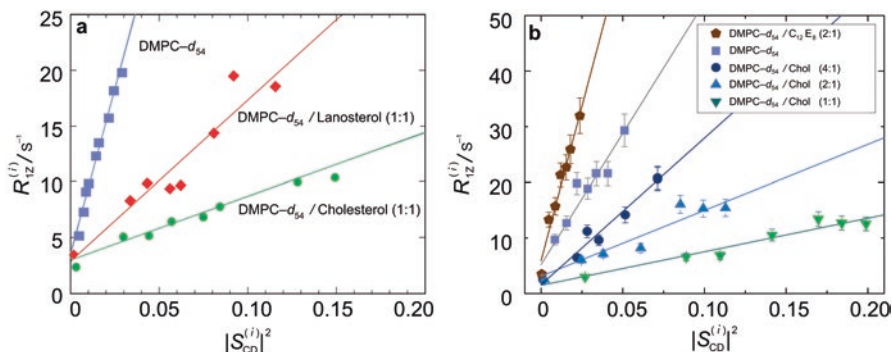
Fig. 4 Solid-state ^{2}H NMR relaxation shows emergence of membrane elastic fluctuations and their suppression by sterols. Dependence of spin-lattice relaxation rates $R_{1Z}^{(i)}$ on squared order parameters $S_{CD}^{(i)}$ for resolved ^{2}H NMR splittings of: (**a**) DMPC-d_{54} showing influences of lanosterol and cholesterol at $T = 55\ °C$. Note that the decrease in the square-law slopes is consistent with a gradual reduction in bilayer elasticity on going from lanosterol to cholesterol (Adapted from Ref. [84]). (**b**) Binary mixtures of DMPC-d_{54} and cholesterol at different mole ratios. Data were obtained at $T = 44\ °C$ and at 76.8 MHz (11.8 T). (Figure adapted and recolored from Ref. [58] with permission of the American Physical Society)

spin polarization of an incident neutron beam as it exchanges energy with the measured lipid membrane. As a quasi-elastic scattering technique, NSE spectroscopy measures neutron energy changes under high resolution on the order of meV (or k_BT). Therefore, it is well suited for detecting biologically relevant thermal fluctuations in lipid membranes. The molecular motions of the lipids, as well as their collective membrane fluctuations, manifest themselves over a wide length and time scales. The accessible length scales by NSE spectrometers are on the order of 1 to a few 100s of nm, making NSE an outstanding tool to probe crucial membrane fluctuations and collective lipid dynamics. Examples of such motions include bending undulations (asymmetric deformations), breathing modes (symmetric deformations), and diffusive lipid dynamics [85–87]. It is important to note that both molecular fluctuations and collective membrane dynamics are determined by the bilayer physical chemistry [51]. Measuring these different modes of membrane dynamics is essential not only to comprehend the core biophysical properties of cell membranes, but also to develop future biomaterials, therapeutic methods, and functional artificial cells. Indeed, to access selective membrane dynamics over specific spatial and temporal scales, NSE spectroscopy has been successfully utilized in the field of membrane biophysics as we discuss below [11, 87–90].

3.1 Principles of Neutron Spin-Echo Spectroscopy

In neutron spin-echo (NSE) spectroscopy, we probe the sample dynamics by utilizing the neutron spin as a timer for the neutron precession within the magnetic field of the spectrometer. This feature enables precise measurement of the energy

exchange between neutrons and the sample during scattering events. Within the magnetic coils of the spectrometer, the Larmor precession of the neutron spin measures the time that each neutron spends in the precession field. This duration of time is directly related to the neutron kinetic energy, or its speed. Thus, by design NSE spectrometers can detect small changes in the neutron energy or speed ($\Delta v/v < 10^{-5}$) as a result of scattering from the sample. Experimentally, these changes are detected as a change in the polarization of the scattered neutron beam [91–93]. Initially, the incoming neutron beam is polarized by a magnetic multilayer mirror, which aligns the spins along the direction of the beam. After that, a $\pi/2$-flipper rotates the spin in the direction perpendicular to the beam axis, i.e., upward. The neutron then enters the first precession coil of length, l, and magnetic field, $\mathbf{B}$, along the neutron beam. The neutron spin undergoes a Larmor precession with the total precession angle, φ, given by the magnetic field integral $J = \int_0^l |\mathbf{B}|\, dx$, where $|\mathbf{B}| = B$ is the modulus of the magnetic induction. The total precession angle is given by: $\varphi = \left(\gamma \lambda m_n/h\right)\int_0^l B\, dx$, where $\gamma = -1.83 \times 10^8$ rad s^{-1} T^{-1} is the gyromagnetic ratio of the neutrons, and $v_n = h/\lambda m_n$ is the neutron velocity, with m_n the neutron mass, h the Planck constant, and λ the neutron wavelength. In NSE spectrometers the change in polarization at the sample position is directly related to the normalized intermediate scattering function, or the dynamic structure factor, $S(\mathbf{Q},t)$, expressed as a function of Fourier time $t = \gamma Bl\hbar/m_n v_n^3$ [91, 94, 95].

Most NSE spectrometers operate with energy resolutions, $\Delta\hbar\omega$, on the order of 10 neV (~100 ns), over length scales on the order of 1–250 Å [93, 96]. Here, $\hbar$ is the reduced Planck constant and ω is the neutron frequency. Notable recent advances in the IN-15 NSE spectrometer at Institut Laue–Langevin have achieved energy resolutions as high as $\Delta\hbar\omega = 0.7$ neV, corresponding to a maximum Fourier time of $t_{max} = 1\mu s$ [97]. These developments allow us to explore even slower dynamics over extended time scales that correspond to crucial membrane processes.

3.2 Membrane Undulations

Membrane fluctuations are key descriptors of the stability and flexibility of membranes, and how they interact with biomacromolecules like cholesterol and proteins. The membrane undulations are dictated by the mechanical properties of the membrane, such as the membrane elasticity, which is determined by the bending rigidity modulus, κ. In early NSE studies the experimental results showed that membrane bending undulations followed the elastic sheet model [98]. Zilman and Granek (ZG) predicted a direct correlation between the NSE relaxation spectra and such membrane undulatory motions. The model is described by stretched exponential decays of the intermediate scattering functions, with a stretched exponent of 2/3, giving a result that reads [99]:

$$S_{ZG}(Q,t) = A\exp\left[-\left(\Gamma_{ZG}t\right)^{2/3}\right]. \tag{7}$$

Here A is the amplitude of the fluctuations, t is the Fourier time, and the parameter Γ_{ZG} is a Q-dependent decay rate, which involves the bending rigidity modulus. For vesicular membranes, such stretched exponential decays have been repeatedly observed in NSE relaxation spectra (Fig. 5a). The corresponding bending rigidity moduli obtained from these measurements are calculated according to theoretical models that leverage refinements of the ZG theory by Watson and Brown [100] to include the interleaflet friction. The resultant expression yields the bending relaxation rates in terms of the effective bending modulus, $\tilde{\kappa}$, which is related to the bilayer bending modulus, κ, by $\tilde{\kappa} = \kappa + 2d^2 k_m$, [100] where k_m is the monolayer area compressibility and d is the distance between the neutral surface and the bilayer midplane. In this derivation, the neutral surface is defined as the membrane surface where the cross-sectional area per lipid molecule remains constant.

Considering the neutral surface to be located at the interface between the hydrophilic headgroup and the hydrophobic lipid tails, the ZG relaxation rates for bending fluctuations can then be expressed as [90, 101]:

$$\frac{\Gamma}{Q^3} = \frac{\Gamma_{ZG}}{Q^3} = 0.0069 \frac{k_B T}{\eta_s} \sqrt{\frac{k_B T}{\kappa}}, \tag{8}$$

where η_s is the solvent viscosity, k_B is the Boltzmann constant, and T is the temperature expressed in K. The Q^3-dependence of Γ_{ZG} is illustrated in Fig. 5b. This approach has become very popular in recent years yielding a direct measurement of membrane mechanics on nanoscopic scales. Accordingly, NSE has been extensively used to determine the bending rigidity moduli κ for various phospholipid membranes, whether in liquid-disordered or in liquid-ordered states [85, 87, 102–109]. Above the gel transition temperature of lipid membranes, the membrane rigidity modulus κ is anticipated to be $\kappa \approx 20\, k_B T$. However, this is highly dependent on the solvent viscosity (as in Eq. 8) [89]. In aqueous buffers the bending rigidity of phospholipid membranes is found to exhibit a linear increase with temperature on approaching the gel transition [90]. When comparing the results with small-angle neutron scattering (SANS) and small-angle X-ray scattering (SAXS) [110], the observations from NSE are generally consistent with the temperature-dependent structural changes in the membrane, marked by a linear increase in the area per lipid with temperature. Combining these results strongly indicates that the membrane elastic properties are strongly dependent on molecular packing of lipids within the membrane. This fundamental structure–property dependence in lipid bilayers was recently validated in NSE studies on membranes of binary lipid mixtures. This study further illustrated that not only the membrane bending rigidity, but also the area compressibility modulus and membrane viscosity, scale with the area per lipid [111].

In another independent investigation on the effect of cholesterol on unsaturated DOPC lipid membranes, Chakraborty et al. [11] demonstrated that on the length and time scales accessible by NSE, cholesterol stiffens the membranes consistent with an increase in molecular packing in DOPC bilayers. This finding is in contrast
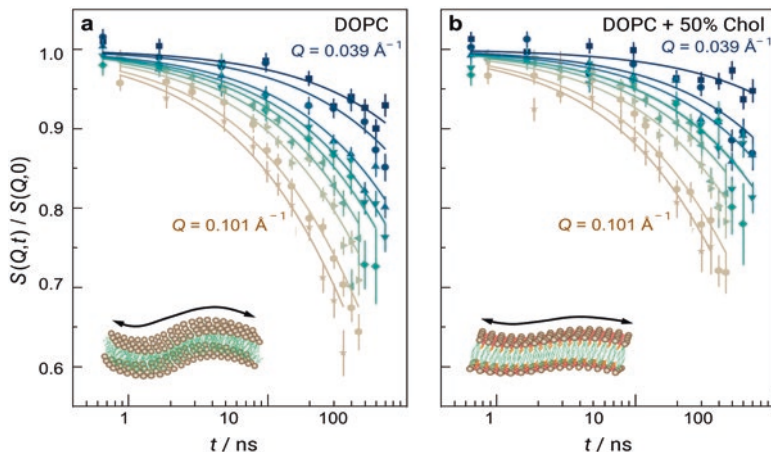
Fig. 5 Exponential decays observed in neutron spin-echo relaxation spectra of vesicular membranes capture membrane dynamics. (**a**) Normalized intermediate scattering functions, $S(Q,t)/S(Q,0)$, of DOPC liposomal membranes with 0 and 50 mol% cholesterol, along with stretched exponential fits (solid lines) given by Eq. (7). (**b**) The decrease in decays in DOPC/cholesterol membranes indicates slowdown in the measured dynamics. (Figure is adapted from Chakraborty et al. [11])

with previous studies on DOPC/cholesterol membranes that have reported no significant changes in membrane rigidity even at cholesterol concentrations of up to 50 mol% [45, 112]. The NSE results from Chakraborty et al. [11] are depicted in Fig. 5 and illustrate the normalized intermediate scattering functions, $S(Q,t)/S(Q,0)$, on DOPC with 0 and 50 mol% cholesterol. The solid lines are the ZG fits of the data as given by Eq. (7). The corresponding Q-dependence of the decay rates is shown in Fig. 6a, illustrating the classic Q^3 signature of bending fluctuations. In Fig. 6a, the shallower slopes are visible for cholesterol-containing membranes, indicating an increased stiffness since the slope for Γ versus Q^3 is $\propto \sqrt{1/\kappa}$. Chakraborty et al. further demonstrated that the bending rigidity modulus scales with the area per lipid, in accord with the increase in molecular packing with increasing cholesterol mole fraction [11]. The study thus demonstrates a direct correlation between the membrane bending rigidity modulus and structural membrane parameters in the form of molecular packing (Fig. 6b). Independently, the same deductions were obtained by solid-state deuterium NMR relaxometry [52] and real-space fluctuation (RSF) analysis by MD simulations [113, 114].

Analogous observations were reported earlier in another NSE investigation on asymmetric saturated and unsaturated POPC lipid membranes mixed with cholesterol [102, 115]. To measure the bending rigidity and intermonolayer friction for different cholesterol content on large unilamellar vesicles (LUV), NSE and dynamic light scattering were combined. It was concluded that due to structural condensation caused by hydrogen-bonding complexes between POPC and cholesterol, a stiffening of POPC membranes in the presence of cholesterol was observed [115]. These
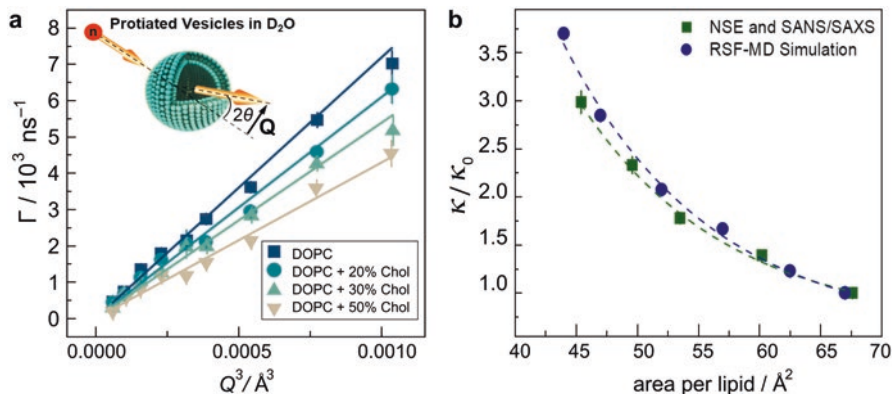
Fig. 6 Increased bending rigidity modulus corresponds to increase in molecular packing with greater cholesterol mole fraction. (**a**) The Q-dependence of the decay rates $\Gamma(Q)$ follows the Q^3 behavior predicted by Zilman and Granek for bending undulations. (**b**) Fits of the decay rates to Eq. (8) yield the bending rigidity moduli, κ. The plots of κ versus area per lipid illustrate dependence of membrane mechanics on the molecular packing as obtained from SANS/SAXS studies. These results are further confirmed by real-space fluctuation (RSF) analysis of atomistic molecular dynamics (MD) simulations. (Figure is adapted from Chakraborty et al. [11])

results follow similar trends as observed for DOPC bilayers. Therefore, all these experiments involving interrogations of the membrane dynamics over similar length and time scales emphasize the universality of the structure–property relationship observed in cholesterol-containing phospholipids.

3.3 How Does the Membrane Thickness Fluctuate?

Membrane thickness fluctuations constitute a collective membrane deformation mode that can be accessed using NSE spectroscopy through selective lipid deuteration. Early predictions of thickness fluctuations, or breathing modes, in lipid membranes came out in the 1980s [116–119]. This crucial dynamic mode has been associated with vital biological membrane processes, such as pore formation [120, 121], as well as passive membrane permeation [122]. The first NSE realizations of membrane thickness fluctuations were obtained on liposomal membranes with chain-deuterated phospholipids [87]. To achieve this finding, NSE experiments were specifically performed at the length scale of the membrane thickness and utilizing the isotope-dependent variation in the neutron scattering length density. The neutron scattering lengths of the protium and deuterium isotopes of hydrogen are −3.74 fm and +6.67 fm, respectively. Therefore, when lipid vesicles are dispersed in a deuterated solvent using chain-deuterated variants of the lipids, the neutron contrast difference between the protiated lipid headgroups and the deuterated hydrocarbon tails intensifies the dynamic NSE signal from variations in the membrane

thickness. Measurements of the long-proposed membrane thickness fluctuation mode were made by exploiting neutron contrast-matching experiments, the most powerful tool in the neutron scattering arsenal. In a similar vein, Chakraborty et al. performed NSE thickness fluctuation measurements on cholesterol-containing di-monounsaturated DOPC lipid membranes [11]. They used acyl chain-perdeuterated DOPC-d_{66}, which was chemically synthesized using deuterated oleic acid, and cholesterol-d_{40}, obtained from genetically modified bacteria to prepare the chain-contrast-matched liposomes. The corresponding SAXS electron density (ED) profiles are illustrated in Fig. 7a, where $z = 0$ indicates the center of the membrane, and $\pm z$ represents the normal distance from the central plane. The electron-rich phosphate groups show peaks in the ED profile as expected. The peak-to-peak distance is defined as the phosphate-to-phosphate thickness, which increases systematically with increasing cholesterol content. The NSE relaxation rates for acyl chain-perdeuterated DOPC-d_{66}/cholesterol membranes are depicted in Fig. 7b, where the lipid chains are contrast-matched with the solvent (^2H_2O). The effect of membrane thickening with increasing cholesterol content is indicated by the peak in the relaxation curves shifting toward decreasing Q-values.

For this kind of contrast-matching experiments, at Q-values corresponding to the membrane thickness, additional heightened dynamics (peak) outside the bending fluctuations are observed (Fig. 7b). In agreement with these results, heightened dynamics have also been observed by ultra-coarse-grained molecular dynamics (MD) simulations [123] for the same-size liposomes. Following the formalism developed by Nagao et al. [90], membrane fluctuations data can be modeled to connect the amplitude and rate of the fluctuations to biophysical membrane parameters, such as the membrane viscosity and area compressibility modulus. This model has been developed based on the theoretical framework by Bingham et al. [124]. Therefore, the thickness fluctuation signal is given by:

$$\frac{\Gamma}{Q^3} = \frac{\Gamma_{ZG}}{Q^3} + \frac{K_A k_B T}{\mu Q_0^3 k_B T + 4 \mu Q_0 K_A A_0 \left(Q - Q_0\right)^2}, \tag{9}$$

where Q_0 is the peak Q-value obtained from SANS, μ is the internal membrane bilayer viscosity, and K_A is the area compressibility modulus obtained from the NSE bending rigidity measurements. It should be noted that here the membrane viscosity, μ, is the only fitting parameter in Eq. (9). Chakraborty et al. [11] used this approach to explore the effect of cholesterol on membrane viscosity. They performed the NSE experiments on DOPC-d_{66} membranes with 0, 10, and 20 mol% of cholesterol-d_{40} [11], illustrating the increase in membrane viscosity with increased cholesterol content (Fig. 7c).

It should be pointed out that using Eq. (9) to obtain the viscoelastic behavior of the membrane requires explicit understanding of the correlation between area compressibility and bending rigidity. Using the elastic thin-sheet deformation model [125], the bending rigidity modulus, κ, has been found to be proportional to the area compressibility modulus, K_A, according to $\kappa = K_A t_m^2 / \varsigma$, where t_m is the mechanical
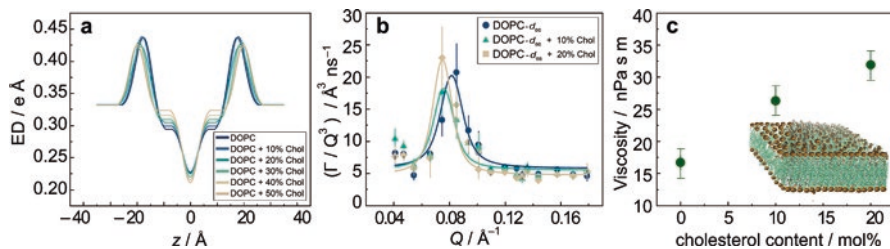
Fig. 7 Small-angle neutron scattering data from selectively deuterated liposomes reveal influences of cholesterol. (**a**) Electron density (ED) profiles along the membrane normal (z-axis) as obtained from SAXS data on DOPC/cholesterol membranes. Here $z = 0$ indicates the central plane of the membrane. The two peaks represent the location of the electron-rich phosphate groups in the membrane bilayer structure. (**b**) NSE relaxation rates measured using tail-perdeuterated DOPC/cholesterol membranes in deuterated buffer solution. Besides the Q^3 signal from bending relaxation, there are additional dynamics attributable to thickness fluctuations as evident by the Lorentzian curve. (**c**) Membrane viscosity calculated from fits of the thickness fluctuations (using Eq. 9) showing greater membrane viscosity with increasing mol% cholesterol. (Figure is adapted from Chakraborty et al. [11])

(or deformable) membrane thickness, and ζ is a constant describing the interleaflet coupling. Within the polymer brush model, $\zeta = 24$ for lightly coupled leaflets, which is typical for lipid membranes in fluid states [125]. Notably, Pan et al. [47] have proposed that for cholesterol-containing unsaturated lipid membranes the polymer brush model does not hold. On the other hand, using MD simulations and a modified assignment of the mechanical membrane thickness, Doktorova et al. [48] have concluded that for a wide range of membrane types, specifically for unsaturated lipid membranes containing cholesterol, the polymer brush model indeed holds. Chakraborty et al. [11] have used this modified polymer brush model to compare the membrane rigidity of completely protiated DOPC to that of the area compressibility modulus of chain-contrast-matched DOPC lipids. They reported that an increase in cholesterol content systematically causes an increase in membrane viscosity. Similar to the observation made by NSE, solid-state ^{2}H NMR experiments likewise yield an increase in the bending rigidity modulus. Taken together, the NSE and solid-state NMR experiments point toward a universal membrane stiffening effect of cholesterol over analogous length and time scales.

4   Biophysical Conclusions and Outlook

The specific chemical interactions of cholesterol and PIP2 with lipid membranes are of great importance for biological function. In this chapter we have reviewed the effects of cholesterol-induced nonspecific material properties with regard to membrane deformation and lipid–protein interactions. However, there is still a gap in the effects of PIP2 and cholesterol on nonspecific material properties of lipid membranes that must be filled to unravel their synergistic influences on cellular

membrane mechanics. Current research indicates the simultaneous increase in cholesterol-induced molecular packing, membrane viscosity, and bending rigidity [11] that entails a suppression of elastic fluctuations at the molecular level, changing the local viscoelastic properties of both saturated and unsaturated membrane bilayers. For lipid membranes investigated by neutron spin-echo measurements [102, 115] and solid-state ^{2}H NMR spectroscopy [52, 126], similar findings have been reported. We can thus draw a clear correlation suggesting an overall increase in membrane rigidity and molecular packing due to interactions with cholesterol. These findings have significant implications for the role of cholesterol in drug incorporation into cell membranes, and in formulating stable liposomes for leak-proof stable drug delivery. This aspect is crucial for the development of next-generation drugs and for studying their effects on live-cell membranes with different cholesterol contents. Stiffening of membranes by cholesterol also impacts our understanding of viral infections, including the recent coronavirus SARS-CoV-2 pandemic. One expects that the fusion, maturation, and budding of viral particles closely depend on the mechanical properties of contact membrane sites, determined by their lipidic and cholesterol content. Investigating the synergism of cholesterol with PIP2 on the regulation of membrane lipid properties is an important future direction that will foster our understanding of phosphoinositide intracellular functions.

References

1. Janmey PA, Lindberg U. Cytoskeletal regulation: rich in lipids. Nat Rev Mol Cell Biol. 2004;5:658–66.
2. Mouritsen OG, Zuckermann MJ. What's so special about cholesterol? Lipids. 2004;39:1101–13.
3. Krause MR, Regen SL. The structural role of cholesterol in cell membranes: from condensed bilayers to lipid rafts. Acc Chem Res. 2014;47:3512–21.
4. Simons K, Ikonen E. How cells handle cholesterol. Science. 2000;290:1721–6.
5. Craig M, Yarrarapu SNS, Dimri M. Biochemistry, cholesterol. Treasure Island: StatPearls Publishing LLC; 2021.
6. Brown MF. Modulation of rhodopsin function by properties of the membrane bilayer. Chem Phys Lipids. 1994;73:159–80.
7. Brown MF. Curvature forces in membrane lipid-protein interactions. Biochemistry. 2012;51:9782–95.
8. Brown MF. Soft matter in lipid–protein interactions. Annu Rev Biophys. 2017;46:379–410.
9. Sheng R, Chen YH, Gee HY, Stec E, Melowic HR, Blatner NR, et al. Cholesterol modulates cell signaling and protein networking by specifically interacting with PDZ domain-containing scaffold proteins. Nat Commun. 2012;3:1–9.

10. Liu S-L, Sheng R, Jung JH, Wang L, Stec E, O'Connor MJ, et al. Orthogonal lipid sensors identify transbilayer asymmetry of plasma membrane cholesterol. Nat Chem Biol. 2017;13:268–74.

11. Chakraborty S, Doktorova M, Molugu TR, Heberle FA, Scott HL, Dzikovski B, et al. How cholesterol stiffens unsaturated lipid membranes. Proc Natl Acad Sci U S A. 2020;117:21896–905.

12. Ashkar R, Doktorova M, Heberle FA, Scott HL, Barrera F, Katsaras J, et al. Reply to Nagle et al.: the universal stiffening effects of cholesterol on lipid membranes. Proc Natl Acad Sci U S A. 2021;118:e2102845118.

13. Scala CD, Baier CJ, Evans LS, Williamson PTF, Fantini J, Barrantes FJ. Relevance of CARC and CRAC cholesterol-recognition motifs in the nicotinic acetylcholine receptor and other membrane-bound receptors. Curr Top Membr. 2017;80:3–23.

14. Paila YD, Chattopadhyay A. Membrane cholesterol in the function and organization of G-protein coupled receptors. In: Harris J, editor. Cholesterol binding and cholesterol transport proteins: subcellular biochemistry. 51. Dordrecht: Springer; 2010. p. 439–66.

15. Kumar GA, Sarkar P, Stepniewski TM, Jafurulla M, Singh SP, Selent J, et al. A molecular sensor for cholesterol in the human serotonin$_{1A}$ receptor. Sci Adv. 2021;7:eabh2922.

16. Zasloff M. Antimicrobial peptides of multicellular organisms. Nature. 2002;415:389–95.

17. Sun F, Schroer CFE, Xu L, Yin H, Marrink SJ, Luo S-Z. Molecular dynamics of the association of L-selectin and FERM regulated by PIP2. Biophys J. 2018;114:1858–68.

18. Singer SJ, Nicolson GL. The fluid mosaic model of the structure of cell membranes. Science. 1972;175:720–31.

19. Fried SDE, Lewis JW, Szundi I, Martínez-Mayorga K, Mahalingam M, Vogel R, et al. Membrane curvature revisited – the archetype of rhodopsin studied by time-resolved electronic spectroscopy. Biophys J. 2021;120:440–52.

20. Brown MF. Influence of nonlamellar forming lipids on rhodopsin. Curr Top Membr. 1997;44:285–356.

21. Brown D, London E. Functions of lipid rafts in biological membranes. Annu Rev Cell Dev Biol. 1998;14:111–36.

22. Simons K, Gerl MJ. Revitalizing membrane rafts: new tools and insights. Nat Rev Mol Cell Biol. 2010;11:688–99.

23. Klose C, Surma MA, Simons K. Organellar lipidomics–background and perspectives. Curr Opin Cell Biol. 2013;25:406–13.

24. Zhang X, Barraza KM, Beauchamp JL. Cholesterol provides nonsacrificial protection of membrane lipids from chemical damage at air–water interface. Proc Natl Acad Sci U S A. 2018;115:3255–60.

25. Auger M, Jarrell HC, Smith IC. Interactions of the local anesthetic tetracaine with membranes containing phosphatidylcholine and cholesterol: a ^{2}H NMR study. Biochemistry. 1988;27:4660–7.

26. Siminovitch DJ, Brown MF, Jeffrey KR. ^{14}N NMR of lipid bilayers: effects of ions and anesthetics. Biochemistry. 1984;23:2412–20.

27. Maxfield FR, van Meer G. Cholesterol, the central lipid of mammalian cells. Curr Opin Cell Biol. 2010;22:422–9.

28. Corvera E, Mouritsen OG, Singer MA, Zuckermann MJ. The permeability and the effect of acyl-chain length for phospholipid bilayers containing cholesterol: theory and experiment. Biochim Biophys Acta. 1992;1107:261–70.

29. Cornelius F. Modulation of Na,K-ATPase and Na-ATPase activity by phospholipids and cholesterol. I. Steady-state kinetics. Biochemistry. 2001;40:8842–51.

30. de Meyer FJM, Rodgers JM, Willems TF, Smit B. Molecular simulation of the effect of cholesterol on lipid-mediated protein-protein interactions. Biophys J. 2010;99:3629–38.

31. Sun X, Whittaker GR. Role for influenza virus envelope cholesterol in virus entry and infection. J Virol. 2003;77:12543–51.

32. Prasad VR, Bukrinsky MI. New clues to understanding HIV nonprogressors: low cholesterol blocks HIV trans infection. MBio. 2014;5:e01396–14.

33. Meher G, Bhattacharjya S, Chakraborty H. Membrane cholesterol modulates oligomeric status and peptide-membrane interaction of severe acute respiratory syndrome coronavirus fusion peptide. J Phys Chem B. 2019;123:10654–62.

34. Kwik J, Boyle S, Fooksman D, Margolis L, Sheetz MP, Edidin M. Membrane cholesterol, lateral mobility, and the phosphatidylinositol 4,5-bisphosphate-dependent organization of cell actin. Proc Natl Acad Sci U S A. 2003;100:13964–9.

35. Hao M, Bogan JS. Cholesterol regulates glucose-stimulated insulin secretion through phosphatidylinositol 4,5-bisphosphate. J Biol Chem. 2009;284:29489–98.

36. Chun YS, Shin S, Kim Y, Cho H, Park MK, Kim T, et al. Cholesterol modulates ion channels via down-regulation of phosphatidylinositol 4,5-bisphosphate. J Neurochem. 2010;112:1286–94.

37. Epand RM. Proteins and cholesterol-rich domains. Biochim Biophys Acta. 2008;1778:1576–82.

38. McLaughlin S, Wang J, Gambhir A, Murray D. PIP(2) and proteins: interactions, organization, and information flow. Annu Rev Biophys Biomol Struct. 2002;31:151–75.

39. Shukla S, Jin R, Robustelli J, Zimmerman ZE, Baumgart T. PIP2 reshapes membranes through asymmetric desorption. Biophys J. 2019;117:962–74.

40. Jiang W, Lin Y, Luo YL. Mechanical properties of anionic asymmetric bilayers from atomistic simulations. J Chem Phys. 2021;154:224701.

41. Duwe HP, Kaes J, Sackmann E. Bending elastic-moduli of lipid bilayers – modulation by solutes. J Phys. 1990;51:945–62.

42. Bassereau P, Sorre B, Lévy A. Bending lipid membranes: experiments after W. Helfrich's model. Adv Colloid Interf Sci. 2014;208:47–57.

43. Dimova R. Recent developments in the field of bending rigidity measurements on membranes. Adv Colloid Interf Sci. 2014;208:225–34.

44. Evans E, Rawicz W. Entropy-driven tension and bending elasticity in condensed-fluid membranes. Phys Rev Lett. 1990;64:2094–7.

45. Gracià RS, Bezlyepkina N, Knorr RL, Lipowsky R, Dimova R. Effect of cholesterol on the rigidity of saturated and unsaturated membranes: fluctuation and electrodeformation analysis of giant vesicles. Soft Matter. 2010;6:1472–82.

46. Niggemann G, Kummrow M, Helfrich W. The bending rigidity of phosphatidylcholine bilayers: dependences on experimental method, sample cell sealing and temperature. J Phys II (Paris). 1995;5:413–25.

47. Pan J, Tristram-Nagle S, Nagle JF. Effect of cholesterol on structural and mechanical properties of membranes depends on lipid chain saturation. Phys Rev E. 2009;80:021931.

48. Doktorova M, LeVine MV, Khelashvili G, Weinstein H. A new computational method for membrane compressibility: bilayer mechanical thickness revisited. Biophys J. 2019;116:487–502.

49. Khelashvili G, Kollmitzer B, Heftberger P, Pabst G, Harries D. Calculating the bending modulus for multicomponent lipid membranes in different thermodynamic phases. J Chem Theory Comput. 2013;9:3866–71.

50. Johner N, Mondal S, Morra G, Caffrey M, Weinstein H, Khelashvili G. Protein and lipid interactions driving molecular mechanisms of in meso crystallization. J Am Chem Soc. 2014;136:3271–84.

51. Brown MF, Ribeiro AA, Williams GD. New view of lipid bilayer dynamics from ^{2}H and ^{13}C NMR relaxation time measurements. Proc Natl Acad Sci U S A. 1983;80:4325–9.

52. Molugu TR, Brown MF. Cholesterol-induced suppression of membrane elastic fluctuations at the atomistic level. Chem Phys Lipids. 2016;199:39–51.

53. Arriaga LR, López-Montero I, Orts-Gil G, Farago B, Hellweg T, Monroy F. Fluctuation dynamics of spherical vesicles: frustration of regular bulk dissipation into subdiffusive relaxation. Phys Rev E. 2009;80:031908.

54. Baumgart T, Capraro BR, Zhu C, Das SL. Thermodynamics and mechanics of membrane curvature generation and sensing by proteins and lipids. Annu Rev Phys Chem. 2011;62:483–506.

55. Molugu TR, Lee S, Brown MF. Concepts and methods of solid-state NMR spectroscopy applied to biomembranes. Chem Rev. 2017;117:12087–132.

56. Reif B, Ashbrook SE, Emsley L, Hong M. Solid-state NMR spectroscopy. Nat Rev Methods Primers. 2021;1:2.

57. Brown MF, Chan SI. Bilayer membranes: deuterium & carbon-13 NMR. In: Grant DM, Harris RK, editors. Encyclopedia of nuclear magnetic resonance. New York: Wiley; 1996. p. 871–85.

58. Martinez GV, Dykstra EM, Lope-Piedrafita S, Job C, Brown MF. NMR elastometry of fluid membranes in the mesoscopic regime. Phys Rev E. 2002;66:050902.

59. Rose ME. Elementary theory of angular momentum. New York: Wiley; 1957.

60. Brown MF. Membrane structure and dynamics studied with NMR spectroscopy. In: Merz Jr KM, Roux B, editors. Biological membranes a molecular perspective from computation and experiment. Basel: Birkhäuser; 1996. p. 175–252.

61. Leftin A, Xu X, Brown MF. Phospholipid bilayer membranes: deuterium and carbon-13 NMR spectroscopy. eMagRes. 2014;3:199–214.

62. Xu X, Struts AV, Brown MF. Generalized model-free analysis of nuclear spin relaxation experiments. eMagRes. 2014;3:275–86.

63. Brown MF. Unified picture for spin-lattice relaxation of lipid bilayers and biomembranes. J Chem Phys. 1984;80:2832–6.

64. Nevzorov AA, Brown MF. Dynamics of lipid bilayers from comparative analysis of ^{2}H and ^{13}C nuclear magnetic resonance relaxation data as a function of frequency and temperature. J Chem Phys. 1997;107:10288–310.

65. Nagle JF, Tristram-Nagle S. Structure of lipid bilayers. Biochim Biophys Acta. 2000;1469:159–95.

66. Brown MF, Thurmond RL, Dodd SW, Otten D, Beyer K. Composite membrane deformation on the mesoscopic length scale. Phys Rev E. 2001;64:010901.

67. Brown MF, Seelig J. Influence of cholesterol on the polar region of phosphatidylcholine and phosphatidylethanolamine bilayers. Biochemistry. 1978;17:381–4.

68. Trouard TP, Nevzorov AA, Alam TM, Job C, Zajicek J, Brown MF. Influence of cholesterol on dynamics of dimyristoylphosphatidylcholine as studied by deuterium NMR relaxation. J Chem Phys. 1999;110:8802–18.

69. Kinnun JJ, Mallikarjunaiah KJ, Petrache HI, Brown MF. Elastic deformation and area per lipid of membranes: atomistic view from solid-state deuterium NMR spectroscopy. Biochim Biophys Acta. 2015;1848:246–59.

70. Bartels T, Bittman R, Beyer K, Brown MF. Raft-like mixtures of sphingomyelin and cholesterol investigated by solid-state ^{2}H NMR spectroscopy. J Am Chem Soc. 2008;130:14521–32.

71. Brzustowicz MR, Cherezov V, Caffrey M, Stillwell W, Wassall SR. Molecular organization of cholesterol in polyunsaturated membranes: microdomain formation. Biophys J. 2002;82:285–98.

72. Shaikh SR, Cherezov V, Caffrey M, Soni SP, LoCascio D, Stillwell W, et al. Molecular organization of cholesterol in unsaturated phosphatidylethanolamines: X-ray diffraction and solid state ^{2}H NMR reveal differences with phosphatidylcholines. J Am Chem Soc. 2006;128:5375–83.

73. Wassall SR, Brzustowicz MR, Shaikh SR, Cherezov V, Caffrey M, Stillwell W. Order from disorder, corralling cholesterol with chaotic lipids. The role of polyunsaturated lipids in membrane raft formation. Chem Phys Lipids. 2004;132:79–88.

74. Brown MF. Deuterium relaxation and molecular dynamics in lipid bilayers. J Magn Reson. 1979;35:203–15.

75. Brown MF, Thurmond RL, Dodd SW, Otten D, Beyer K. Elastic deformation of membrane bilayers probed by deuterium NMR relaxation. J Am Chem Soc. 2002;124:8471–84.

76. Nevzorov AA, Trouard TP, Brown MF. Lipid bilayer dynamics from simultaneous analysis of orientation and frequency dependence of deuterium spin-lattice and quadrupolar order relaxation. Phys Rev E. 1998;58:2259–81.

77. Althoff G, Frezzato D, Vilfan M, Stauch O, Schubert R, Vilfan I, et al. Transverse nuclear spin relaxation studies of viscoelastic properties of membrane vesicles. I. Theory. J Phys Chem B. 2002;106:5506–16.

78. Althoff G, Stauch O, Vilfan M, Frezzato D, Moro GJ, Hauser P, et al. Transverse nuclear spin relaxation studies of viscoelastic properties of membrane vesicles. II. Experimental results. J Phys Chem B. 2002;106:5517–26.

79. Bloom M, Evans E. Observations of surface undulations on the mesoscopic length scale by NMR. In: Peliti L, editor. Biologically inspired physics. New York: Plenum; 1991. p. 137–47.

80. Bloom M, Evans E, Mouritsen OG. Physical properties of the fluid lipid-bilayer component of cell membranes: a perspective. Q Rev Biophys. 1991;24:293–397.

81. Molugu TR, Lee SK, Job C, Brown MF. Hydration-modulated collective dynamics of membrane lipids are revealed by solid-state ^{2}H NMR relaxation. Biophys J. 2015;108:77a.

82. Molugu TR, Lee S, Xu X, Mallikarjunaiah KJ, Job C, Brown MF. Emergence of undulations as 2-D director fluctuations in phospholipid membranes. Biophys. J. 2018;114: 391a-392a.

83. Brown MF. Theory of spin-lattice relaxation in lipid bilayers and biological membranes. ^{2}H and ^{14}N quadrupolar relaxation. J Chem Phys. 1982;77:1576–99.

84. Martinez GV, Dykstra EM, Lope-Piedrafita S, Brown MF. Lanosterol and cholesterol-induced variations in bilayer elasticity probed by ^{2}H NMR relaxation. Langmuir. 2004;20:1043–6.

85. Gupta S, De Mel JU, Schneider GJ. Dynamics of liposomes in the fluid phase. Curr Opin Colloid Interface Sci. 2019;42:121–36.

86. Katsaras J, Gutberlet T. Lipid bilayers: structure and interactions. Berlin/Heidelberg: Springer; 2001.

87. Woodka AC, Butler PD, Porcar L, Farago B, Nagao M. Lipid bilayers and membrane dynamics: insight into thickness fluctuations. Phys Rev Lett. 2012;109:058102.

88. Ashkar R, Nagao M, Butler PD, Woodka AC, Sen MK, Koga T. Tuning membrane thickness fluctuations in model lipid bilayers. Biophys J. 2015;109:106–12.

89. Gupta S, De Mel JU, Perera RM, Zolnierczuk P, Bleuel M, Faraone A, et al. Dynamics of phospholipid membranes beyond thermal undulations. J Phys Chem Lett. 2018;9:2956–60.

90. Nagao M, Kelley EG, Ashkar R, Bradbury R, Butler PD. Probing elastic and viscous properties of phospholipid bilayers using neutron spin echo spectroscopy. J Phys Chem Lett. 2017;8:4679–84.

91. Mezei F. Neutron spin echo: a new concept in polarized thermal neutron techniques. Z Physik. 1972;255:146–60.

92. Mezei F, Pappas C, Gutberlet T. Neutron spin echo spectroscopy basics, trends and applications. Berlin: Springer; 2002.

93. Monkenbusch M, Richter D. High resolution neutron spectroscopy – a tool for the investigation of dynamics of polymers and soft matter. C R Phys. 2007;8:845–64.

94. Ashkar R. Selective dynamics in polymeric materials: insights from quasi-elastic neutron scattering spectroscopy. J Appl Phys. 2020;127:151101.

95. Ohl M, Monkenbusch M, Arend N, Kozielewski T, Vehres G, Tiemann C, et al. The spin-echo spectrometer at the spallation neutron source (SNS). Nucl Instrum Methods Phys Res. 2012;696:85–99.

96. Monkenbusch M, Schatzler R, Richter D. The Jülich neutron spin-echo spectrometer – design and performance. Nucl Instrum Methods Phys Res. 1997;399:301–23.

97. Farago B, Falus P, Hoffmann I, Gradzielski M, Thomas F, Gomez C. The IN15 upgrade. Neutron News. 2015;26:15–7.

98. Yamada LN, Seto H, Takeda T, Nagao M, Kawabata Y, Inoue K. SAXS, SANS and NSE studies on "unbound state" in DPPC/water/CaCl$_2$ system. J Phys Soc Jpn. 2005;74:2853–9.

99. Zilman AG, Granek R. Undulations and dynamic structure factor of membranes. Phys Rev Lett. 1996;77:4788–91.

100. Watson MC, Brown FL. Interpreting membrane scattering experiments at the mesoscale: the contribution of dissipation within the bilayer. Biophys J. 2010;98:L9–L11.

101. Hoffmann I, Michel R, Sharp M, Holderer O, Appavou MS, Polzer F, et al. Softening of phospholipid membranes by the adhesion of silica nanoparticles – as seen by neutron spin-echo (NSE). Nanoscale. 2014;6:6945–52.
102. Arriaga LR, López-Montero I, Monroy F, Orts-Gil G, Hellweg T. Stiffening effect of cholesterol on disordered lipid phases: a combined neutron spin echo + dynamic light scattering analysis of the bending elasticity of large unilamellar vesicles. Biophys J. 2009;96:3629–37.
103. De Mel JU, Gupta S, Perera RM, Ngo LT, Zolnierczuk P, Bleuel M, et al. Influence of external NaCl salt on membrane rigidity of neutral DOPC vesicles. Langmuir. 2020;36:9356–67.
104. De Mel JU, Gupta S, Willner L, Allgaier J, Stingaciu LR, Bleuel M, et al. Manipulating phospholipid vesicles at the nanoscale: a transformation from unilamellar to multilamellar by an *n*-alkyl-poly(ethylene oxide). Langmuir. 2021;37:2362–75.
105. Gupta S, Ashkar R. The dynamic face of lipid membranes. Soft Matter. 2021;7:6910–28.
106. De Mel JU, Gupta S, Harmon S, Stingaciu L, Roth EW, Siebenbuerger M, et al. Acetaminophen interactions with phospholipid vesicles induced changes in morphology and lipid dynamics. Langmuir. 2021;37:9560–70.
107. Gupta S, Schneider GJ. Modeling the dynamics of phospholipids in the fluid phase of liposomes. Soft Matter. 2020;16:3245–56.
108. Lee JH, Choi SM, Doe C, Faraone A, Pincus PA, Kline SR. Thermal fluctuation and elasticity of lipid vesicles interacting with pore-forming peptides. Phys Rev Lett. 2010;105:038101.
109. Sharma VK, Mamontov E, Ohl M, Tyagi M. Incorporation of aspirin modulates the dynamical and phase behavior of the phospholipid membrane. Phys Chem Chem Phys. 2017;19:2514–24.
110. Kučerka N, Nieh MP, Katsaras J. Fluid phase lipid areas and bilayer thicknesses of commonly used phosphatidylcholines as a function of temperature. Biochim Biophys Acta. 2011;1808:2761–71.
111. Kelley EG, Butler PD, Ashkar R, Bradbury R, Nagao M. Scaling relationships for the elastic moduli and viscosity of mixed lipid membranes. Proc Natl Acad Sci U S A. 2020;117:23365–73.
112. Pan J, Mills TT, Tristram-Nagle S, Nagle JF. Cholesterol perturbs lipid bilayers nonuniversally. Phys Rev Lett. 2008;100:198103.
113. Doktorova M, Harries D, Khelashvili G. Determination of bending rigidity and tilt modulus of lipid membranes from real-space fluctuation analysis of molecular dynamics simulations. Phys Chem Chem Phys. 2017;19:16806–16818.
114. Johner N, Harries D, Khelashvili G. Implementation of a methodology for determining elastic properties of lipid assemblies from molecular dynamics simulations. BMC Bioinform. 2016;17:161.
115. Arriaga LR, Rodríguez-García R, López-Montero I, Farago B, Hellweg T, Monroy F. Dissipative curvature fluctuations in bilayer vesicles: coexistence of pure-bending and hybrid curvature-compression modes. Eur Phys J E. 2010;31:105–13.
116. Bach D, Miller IR. Glyceryl monooleate black lipid membranes obtained from squalene solutions. Biophys J. 1980;29:183–7.
117. Hladky SB, Gruen DW. Thickness fluctuations in black lipid membranes. Biophys J. 1982;38:251–8.
118. Israelachvili JN, Wennerström H. Entropic forces between amphiphilic surfaces in liquids. J Phys Chem. 1992;96:520–31.
119. Miller IR. Energetics of fluctuation in lipid bilayer thickness. Biophys J. 1984;45:643–4.
120. Bennett WF, Sapay N, Tieleman DP. Atomistic simulations of pore formation and closure in lipid bilayers. Biophys J. 2014;106:210–9.
121. Movileanu L, Popescu D, Ion S, Popescu AI. Transbilayer pores induced by thickness fluctuations. J Math Biol. 2006;68:1231–55.
122. Orsia M, Essex JW. Permeability of drugs and hormones through a lipid bilayer: insights from dual-resolution molecular dynamics. Soft Matter. 2010;6:3797–808.

123. Carrillo J-MY, Katsaras J, Sumpter BG, Ashkar R. A computational approach for modeling neutron scattering data from lipid bilayers. J Chem Theory Comput. 2017;13:916–25.
124. Bingham RJ, Smye SW, Olmsted PD. Dynamics of an asymmetric bilayer lipid membrane in a viscous solvent. EPL (Europhys Lett). 2015;111:18004.
125. Rawicz W, Olbrich KC, McIntosh T, Needham D, Evans E. Effect of chain length and unsaturation on elasticity of lipid bilayers. Biophys J. 2000;79:328–39.
126. Martinez GV, Dykstra EM, Lope-Piedrafita S, Job C, Brown MF. Solid state deuterium NMR study of the effects of sterols on membrane elasticity. Biophys J. 2002;82:544a.